Phase Diagrams of Alloys and Their Hydrides via On-Lattice Graph Neural Networks and Limited Training Data

Matthew D. Witman[1,*], Norman C. Bartelt[1,*], Sanliang Ling[2], Pin-Wen Guan[1], Lauren Way[1],
Mark D. Allendorf[1], and Vitalie Stavila[1]

[1]Sandia National Laboratories, Livermore, California 94551, United States

[2]Advanced Materials Research Group, Faculty of Engineering, University of Nottingham,
University Park, Nottingham NG7 2RD, U.K.

[*]*mwitman@sandia.gov*; *bartelt@sandia.gov*

Abstract

Efficient prediction of sampling-intensive thermodynamic properties is needed to evaluate material performance and permit high-throughput materials modeling for a diverse array of technology applications. To alleviate the prohibitive computational expense of high-throughput configurational sampling with density functional theory (DFT), surrogate modeling strategies like cluster expansion are many orders of magnitude more efficient, but can be difficult to construct in systems with high compositional complexity. We therefore employ minimal-complexity graph neural network models that accurately predict, and can even extrapolate to out-of-train-distribution, formation energies of DFT-relaxed structures from an ideal (unrelaxed) crystallographic representation. This enables the large-scale sampling necessary for various thermodynamic property predictions that may otherwise be intractable and can be achieved with small training datasets. Two exemplars, optimizing thermodynamic stability of low-density high entropy alloys and the modulating the plateau pressure of hydrogen in metal alloys, demonstrate the power of this approach, which will be extendable to a variety of materials discovery and modeling problems.

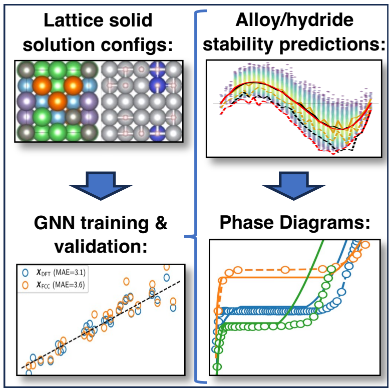

Main Text

Compositionally complex or high entropy alloys[1] have been extensively investigated for a plethora of applications due to their outstanding thermal,[2] mechanical,[3] energy storage,[4–6] and catalytic properties,[7] but rational design of these materials is challenged by the combinatorial explosion of the compositional space from which they can be synthesized. Accurate and tractable modeling strategies[8] are therefore critical for discovering and/or optimizing high entropy alloys[8,9] to direct the synthesis and testing of promising materials and conserve expensive experimental resources.[10] Crucially, any modeling approach must be accurate and data-efficient in treating solid solutions with high compositional complexity. Another critical consideration is that the model's input needs to be trivial-to-generate such that hundreds of thousands or millions of energy calculations can then be performed. This enables convergence of materials' property predictions through first principles simulations like Monte Carlo or direct statistical sampling.[11]

The introduction of the cluster expansion (CE) method[12] often satisfies the aforementioned requirements and its initial applications in the prediction of phase stability of complex alloys[13,14] marked a significant milestone in the ability to rationally design complex inorganic materials and impact a host of technological applications. Its widespread popularity mainly stems from its ability to accurately predict complex energy landscapes in materials exhibiting significant configurational degrees

---

‡ *Supporting Information*: details on density functional theory calculations, graph neural network training, thermodynamic calculations, and experimental PCT measurements.

of freedom while requiring only a relatively small (or at least tractable) number of expensive first-principles electronic structure calculations. The cluster expansion formalism has enabled first-principles accuracy calculations of temperature-composition phase diagrams,[15] activation barriers,[16,17] and even electronic excitations[18] across diverse materials applications, ranging from hydrogen storage[19] to battery[20] to electronic device materials.[21] Furthermore, along with the recent explosion of machine learning (ML) to accelerate various tasks in materials science, ML improvements on the original cluster expansion formalism have been proposed to ameliorate some of its shortcomings.[22–24]

Parallely, in recent years, graph neural networks (GNNs)[25–29] have undergone widespread adoption in materials science thanks to their automated feature extraction capabilities. They generally remove the need to manually derive input features (e.g., the process of defining the cluster functions in CE) that suitably describe a material of high compositional complexity. They can serve as direct surrogate models for highly demanding computational tasks (e.g., bulk modulus and equation-of-state fitting,[30,31] supercell defect relaxations,[32] or phonon density of state calculations[33]) and more recently have been developed towards "universal" force fields to enable first-principles accuracy simulations across the periodic table.[34,35] Here we demonstrate how minimal-complexity GNNs (i.e., ∼2,000 parameter models) with identical architectures and training hyperparameters are applicable to *relaxed* formation energy predictions from *un-relaxed* crystallographic representations to aid the design of compositionally complex materials with limited training data. For example, this approach permits the high-throughput screening needed to predict and therefore compositionally optimize phase stability of low density high-entropy alloys and hydrogen equilibria in metal hydrides. Critically, these models' predictions extrapolate to configurations with formation energies outside the range of target values in the training data, and small training datasets can be rationally and efficiently constructed to maximize performance. In the future, we expect such an approach to be useful in any number of applications that CE has typically been used to study, while alleviating challenges of constructing cluster functions in high compositional complexity systems.

Graph neural networks on ideal lattices. High-throughput configurational sampling is often needed for thermodynamic property predictions in solid solution materials; therefore, a DFT surrogate model that can predict, for example, relaxed formation energies from a trivial-to-generate crystallographic representation is critical. In the case of the cubic FCC lattice (or BCC, HCP, etc.), the idealized crystal representation, X_{FCC}, is defined by the elemental identify of each lattice site at its ideal fractional coordinate (Figure 1). The energy of the DFT-relaxed crystal structure, X_{DFT}, with respect to possible decomposition products yields the desired prediction target: the formation energy, $E_{f,\mathrm{DFT}}$. A useful model for ML-accelerated calculation of thermodynamic properties must utilize X_{FCC} as input (if X_{DFT} is known, then so is $E_{f,\mathrm{DFT}}$ and the model is moot).

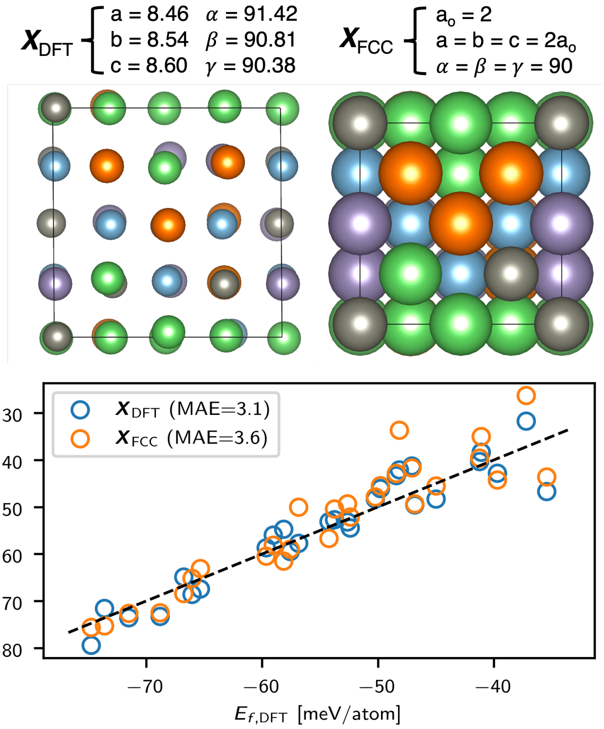

Figure 1: Parity plot for test set predictions of relaxed formation energy from a model trained on the DFT-relaxed crystal structures (X_{DFT}) vs. a model trained on structures mapped back to the idealized FCC lattice (X_{FCC}).

Therefore we seek a GNN model, f_{GNN}, parameterized by optimized weights θ, that predicts the formation energy,

$$\hat{E}_f = f_{\mathrm{GNN}}(X_{\mathrm{FCC}}; \theta), \tag{1}$$

where the idealized lattice in this example is X_{FCC}. Despite the continually expanding plethora of GNN variants,[25–29] we utilize CGCNN[25] due to its comparative simplicity and ability to construct models with low architecture complexity and a relatively small number of trainable parameters (see Supplementary Section 2 for details). For a simple test case, we generate a database of 284 random X_{FCC} configurations with an equimolar AlLiMgSnZn stoichiometry (the synthesis target of Ref. [10]), DFT optimize (Supplementary Section 1) their geometries to obtain X_{DFT} and $E_{f,\mathrm{DFT}}$, and map X_{DFT} back to X_{FCC}. Figure 1 summarizes both X_{DFT} and X_{FCC} models' test set performance on a 80/10/10 train/validation/test split. Henceforth referred to as Model 1, the GNN trained on X_{FCC} inputs still predicts $\hat{E}_f$ with nearly identical accuracy as one trained on X_{DFT}, with a mean absolute error (MAE) of 3.1 vs 3.6 meV/atom. Since X_{DFT} unambiguously maps to X_{FCC} despite local distortions, we can model the relaxed formation enthalpies and perform high-throughput configurational screening by using X_{FCC} as a trivial-to-generate input.

Single-shot compositional optimization of low–density HEAs. The design of low-density alloys has attracted significant attention in structural materials applications,[36] so we utilize our GNN modeling to demonstrate whether one can explain an experimentally inaccessible target[10] (the single-phase FCC solid solution of equimolar AlLiMgSnZn) and improve its thermodynamic synthesizability via compositional optimization. First, Model 1 (from Figure 1) was tested by predicting formation energies ($\hat{E}_{f,\text{M1}}$) of 10,000 random equimolar AlLiMgSnZn and off-equimolar $\text{Al}_{0.5}\text{LiMg}_{0.5}\text{SnZn}_{0.5}$ configurations. This screening both converges the probability distribution of formation energies and predicts significantly out-of-train-distribution values, especially for $\text{Al}_{0.5}\text{LiMg}_{0.5}\text{SnZn}_{0.5}$ (Figure 2a). We re-validate a sampling of these configurations (Figure 2b) to generally demonstrate both the overall model accuracy (MAE = 5.2 and 7.9 meV/atom for AlLiMgSnZn and $\text{Al}_{0.5}\text{LiMg}_{0.5}\text{SnZn}_{0.5}$, respectively) and the accuracy in extrapolating to out-of-train-distribution formation energies.

Next, we screened compositions with greater off-equimolar stoichiometry, i.e., all possible permutations of at. fractions $x \in \{0.5, 1.5\}$, and computed $E_{f,\text{DFT}}$ for the min, median, and max predicted energy configurations for each composition (Figure 2c). With a slope of ∼1 for most compositions, Model 1 predicts relative formation energies of the intra-composition configurations correctly but with a constant error shift that is composition dependent. This yields a lower than desired accuracy with MAE = 41 meV/atom and Pearson correlation coefficient (PCC) = 0.72. To remedy this, $E_{f,\text{DFT}}$ was calculated for the 5 elemental X_{FCC} configurations and four random X_{FCC} configurations for each 2-, 3-, and 4-element equimolar compositions, requiring $5+4\left(\binom{5}{4}+\binom{5}{3}+\binom{5}{2}\right)=105$ new DFT relaxations. With this additional training data, Model 2's predictions, $\hat{E}_{f,\text{M2}}$, achieve significantly improved quantitative accuracy on the same off-equimolar test set in Figure 2d (MAE = 4.4 meV/atom and PCC = 0.99). Model 2 is now sufficiently accurate to quantitatively differentiate formation energies between differing compositions, can be employed for phase stability predictions, and importantly can be derived from in a single-shot execution of DFT relaxations involving at most ∼300-400 training examples.

Synthetic accessibility of a target phase is dependent upon its free energy above the convex hull, E_h,[37] subject to standard assumptions for DFT-computed phase stability and thermodynamic synthesizability limits of metastable phases.[38] $\hat{E}_{h,\text{M2}}$ is computed from $\hat{E}_{f,\text{M2}}$ distributions for select off-equimolar, 5-element compositions using Materials Project data[39] and pymatgen[37] (Figure 2e). Even the minimum E_h configurations, let alone a Boltzmann weighted average across configurations, are near or above the typically assumed values for the upper synthesizability limit for metastable materials (∼0.05-0.10 eV/atom above the hull). The strong thermodynamic driving force for decomposition of the FCC phase is qualitatively consistent with the inability of experiments to isolate single-phase FCC solid solutions in this composition space.[10] The hull energy of the phase diagram is lowered significantly by the highly favorable formation of, for example, Mg_2Sn intermetallic compounds. Therefore, removing Sn and screening $\hat{E}_{f,\text{M2}}$ for (Al,Li,Mg,Zn) compositions, the minimum $\hat{E}_{h,\text{M2}}$ can be reduced by ∼0.04 eV/atom, which remains high but marginally improves potential for synthesizability from a thermodynamic perspective. In the future, FCC training databases with more elements can be developed[40] to enable accurate predictions of more alloying strategies or altogether different composition spaces that can identify candidate low-density high entropy alloys with low or zero E_h.

PCT curve prediction for Pd-alloyed hydrides. The excellent stability and reversible hydrogen absorption of Pd has led to its establishment as a benchmark material in the hydrogen storage community. The ability to model its thermodynamic equilibrium with hydrogen, i.e., the pressure-composition-temperature (PCT) curve, and *a priori* predict the affects of alloying are critical to both practically test any proposed thermodynamic modeling strategy and also inform rational tuning strategies for specific storage applications.[41,42] Now, Equation (1) is modified to account for hydrogen atom occupation of the octahedral interstitial sites, and the idealized crystallographic input to the GNN is a concatenation of the alloyed FCC lattice and the interstitial lattice,

$$\hat{E}_f = f_{\text{GNN}}(X_{\text{FCC}} \oplus X_{\text{interstitials}}; \theta). \qquad (2)$$

Figure 3 first validates the capabilities of Equation (2) to capture the configurational energy landscape of hydrogen absorption in PdH_x, $\text{Pd}_{0.91}\text{Rh}_{0.09}\text{H}_x$, and $\text{Pd}_{0.91}\text{Ag}_{0.09}\text{H}_x$ alloys. Training configurations for $0 < x < 1$, where x is the hydrogen to metal ratio (H/M), were generated by sampling random alloy configurations in the 32 atom FCC supercell and random hydrogen occupation of the octahedral interstitials, with 80 DFT-relaxed configurations per x (Supplementary Section 1). Figure 3a's test set parity plots for 80/10/10 train/validation/test splits demonstrate excellent model performance with MAEs of 0.3, 0.8, 1.1 meV/atom for PdH_x, $\text{Pd}_{0.91}\text{Rh}_{0.09}\text{H}_x$ and $\text{Pd}_{0.91}\text{Ag}_{0.09}\text{H}_x$, respectively. Figure 3b shows train and test set predictions for $\text{Pd}_{0.91}\text{Rh}_{0.09}\text{H}_{0.5}$ alongside several minimum and maximum energies predicted by ML screening 10,000 random configurations, which again demonstrates successful out-of-train-distribution predictions. Finally, Figure 3c shows both histograms of the signed test set errors for

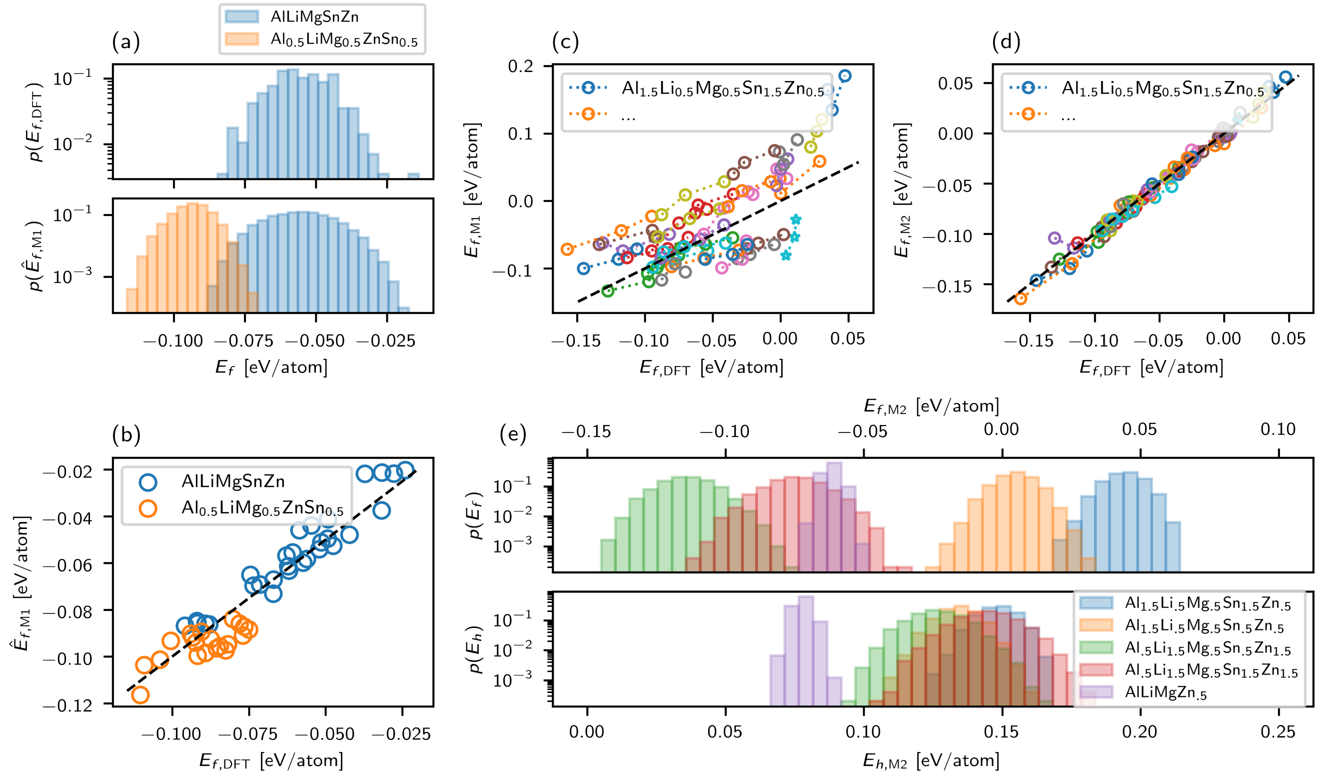

Figure 2: (a) Distribution of $E_{f,\mathrm{DFT}}$ for the 284 random AlLiMgSnZn configuration dataset used to train Model 1 (top) and the distribution of Model 1's predictions, $\hat{E}_{f,\mathrm{M1}}$, from screening 10,000 random configurations per composition (bottom). (b) Validating the screening predictions in panel (a) after computing $E_{f,\mathrm{DFT}}$. (c) The screening of all possible 5-element permutations with atomic fractions $x \in \{0.5, 1.5\}$ with the min, median, and max $\hat{E}_{f,\mathrm{M1}}$ configuration validated after computing $E_{f,\mathrm{DFT}}$. (d) Model 2's predictions, $\hat{E}_{f,\mathrm{M2}}$, on the same configurations as panel (c). (e) Model 2's predicted $\hat{E}_{f,\mathrm{M2}}$ and $\hat{E}_{h,\mathrm{M2}}$ distributions from 5,000 randomly sampled configurations for select compositions.

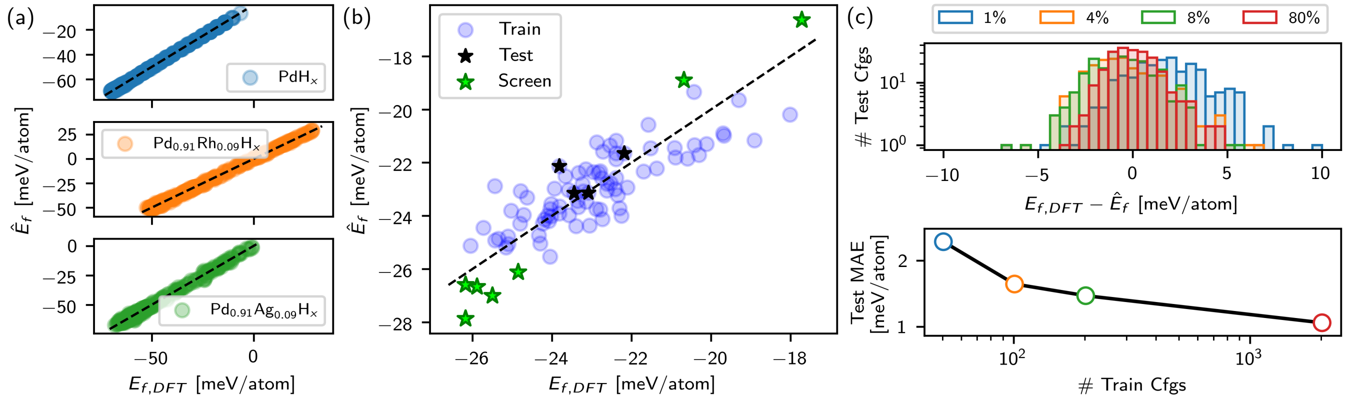

Figure 3: (a) Test set predictions from 80/10/10 train/validation/test split models for Pd, Rh-substituted, and Ag-substituted alloys across all $0 < x < 1$ [H/M] densities. (b) An expanded view of the train and test predictions for the Rh-substituted alloy at a density of $x = 0.5$. Green stars indicate low and high energy configurations discovered by screening 10,000 new configurations at $x = 0.5$ which were subsequently re-tested with DFT. (c) The test set errors for $Pd_{29}Ag_3H_x$ when only 80%, 8%, 4%, or 1% of the train split was utilized for model training.

$Pd_{0.91}Ag_{0.09}H_x$ and the overall test MAE when only 80%, 8%, 4% or 1% of the train split is used for model training. The ML still achieves high performance with a test set MAE of ∼1.5 meV/atom when only ∼100 configura-

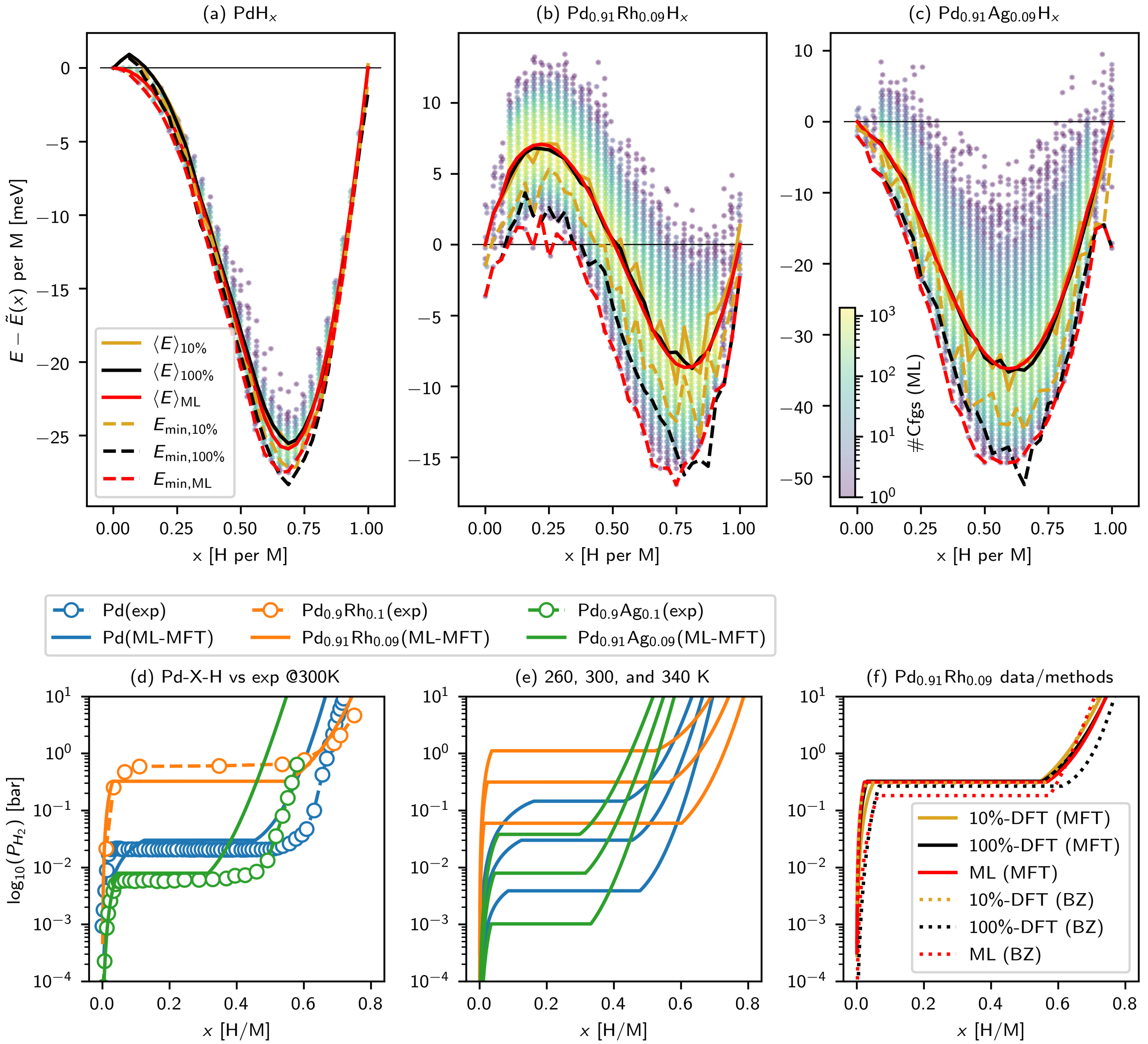

Figure 4: (a-c) ML screened configurational energies for each system are shown in the density plot, as well as $\langle E \rangle(x)$ and $E_{\mathrm{min}}(x)$, for 10% of the training data, 100% of the training data, and the high-throughput ML predictions. (d) Comparison of the MFT PCT curve predictions based on the ML screening with experiments for each system at 300 K. (e) Elucidation of the phase envelope by computing PCT curves at increasing temperatures. (f) Comparison of the PCT curves for Pd$_{0.91}$Rh$_{0.09}$ based on 10% of the training data, 100% of the training data, and the high-throughput ML predictions using either MFT or BZ weighting.

tions are used for training, although the addition of 20x more training data still contributes to significant error reduction.

For $0 < x < 1$ [H/M], we compute formation energies of either 1,000 (for PdH$_x$) or 10,000 (for Pd$_{0.91}$Rh$_{0.09}$H$_x$ and Pd$_{0.91}$Ag$_{0.09}$H$_x$) random configurations per x. Density plots in Figure 4a-c show the ML screened energies, $E(x)$, for each system. A linear interpolation of the average energy between $E(x = 0)$ and $E(x = 1)$, denoted $\tilde{E}(x)$, has been subtracted to better visualize the change in convexity as a function of x. The average energy, $\langle E \rangle(x)$, and minimum energy, $E_{\mathrm{min}}(x)$, are also plotted for a "10%" sampling of the training data, "100%" sampling of the training data, and the full "ML" screening. The narrowly distributed $E(x)$ for PdH$_x$ makes even the "10%" sampling of the training data sufficient to converge $\langle E \rangle(x)$, and $E_{\mathrm{min}}(x)$ within 1 meV per metal of the "ML" screening. However, due to the substantially wider $E(x)$ distribution in the alloyed systems, the "10%" sampling is insufficient to even smoothly converge $\langle E \rangle(x)$, and the

"ML" screening systematically converges the sampling of low energy configurations with several meV/atom lower $E_{\min}(x)$ than the "100%" sampling of the training data.

Finally, PCT curves were computed using either a mean field theory formalism (MFT) or a Boltzmann (BZ) weighting of the energies (Supplementary Section 3) for each alloy system and using the "10%" sampling, "100%" sampling, or the ML screening. Figure 4d demonstrates how this methodology can successfully resolve the ranking of experimental plateau pressures, plateau width, and saturation capacity between the 3 systems. The Pd-hydrogen PCT curve was measured in-house (Supplementary Section 4), while experimental PCT curves for Pd-Rh and Pd-Ag were taken from Ref. [43]. Figure 4e shows how PCT curves can be computed at different temperatures to resolve the phase envelope, i.e., the decrease in plateau width and increase in plateau pressure as a function of increasing temperature. Interestingly, Figure 4f demonstrates that similar PCT curves are computed regardless of data source and methodology in these systems, mainly due the narrowly distributed $E(x)$. We expect the ML-based configurational screening will compound in necessity when moving to higher complexity systems where the energy probability distributions broaden significantly with varying local alloy environments (e.g., Figure 2) and varying strengths of hydrogen binding in more diverse interstitial environments.

Discussion. This work demonstrates the accuracy and transferability of graph neural network models to accurately predict the DFT-relaxed properties (i.e., formation energies) of a crystal structure that has been mapped onto an idealized lattice/interstitial representation. It shares the advantages of the CE method in that (1) only a small number of DFT training examples are needed (∼100s) to obtain meV/atom MAEs in up to quinary composition spaces and (2) model inputs are derived from a trivial-to-generate representation of the relaxed crystal structure. Therefore, one can then rapidly and accurately compute energetics of hundreds of thousands of random alloy configurations that may be needed to converge thermodynamic property predictions. At the same time, we showed how the CGCNN approach employing an identical, low-complexity architecture and identical hyperparameters can accurately predict configurational energetics in diverse materials for diverse applications. This removes the need for manual tuning of the CE method when transitioning between problems of varying complexity.

We have shown meV/atom and sub-meV/atom MAEs, i.e., below the expected error of DFT with respect to experiments,[44] using a limited amount of training data in two different and important practical applications of compositionally complex metals. First, we provided a single-shot learning approach to compositionally optimize the thermodynamic stability of low-density HEAs. The results were used to explain experimental observations in the failed synthesis of a phase pure AlLiMgSnZn solid solution FCC alloy. Our screening found a similar composition that reduces the energy above the hull from ∼100 meV/atom by ∼40 meV/atom and the density. In the second application, we applied our methodology to more structurally intricate FCC hydrides and screened the energy landscape of H occupation in Pd-substituted alloys. To predict the key thermodynamic property for materials-based hydrogen storage, we then calculated the PCT curves with sufficient accuracy (for the first time to our knowledge) to quantitatively capture alloy substitution effects on the plateau pressure, its effect on saturation capacities, and elucidate the phase envelope of the metal to hydride transition. Moving forward, we anticipate this approach to be useful in any variety of inorganic materials applications that have traditionally been investigated by the CE method. Meanwhile, the clear limitation of this approach (and that of CE) occurs if lattice distortions are so great that there is no longer a unique mapping from the DFT-relaxed structure to its ideal lattice configuration, in which case one would likely resort to atomistic potentials and simulations for phase diagram predictions. We envision the build-up of large-scale FCC, BCC, HCP, etc. databases,[40] where the generalizability and flexibility of GNN models can be used for accurate predictions across large compositional spaces without explicitly accounting for, for example, sparsity of the cluster functions in CE. We envision this to impact not only structural alloy and hydride design as demonstrated in this work, but the expansive realm of applications in which high entropy materials are being investigated today.

Acknowledgements

The authors gratefully acknowledge research support from the U.S. Department of Energy, Office of Energy Efficiency and Renewable Energy, Fuel Cell Technologies Office through the Hydrogen Storage Materials Advanced Research Consortium (HyMARC). This work was supported by the Laboratory Directed Research and Development (LDRD) program at Sandia National Laboratories. Sandia National Laboratories is a multimission laboratory managed and operated by National Technology & Engineering Solutions of Sandia, LLC, a wholly owned subsidiary of Honeywell International Inc., for the U.S. Department of Energy's National Nuclear Security Administration (DOE/NNSA) under contract DE-NA0003525. This written work is authored by an employee of NTESS. The employee, not NTESS, owns the right, title and interest in and to the written work and is responsible for its contents. Any subjective views or opinions that might be expressed in the written work do not necessarily represent the views of the U.S. Government. The publisher acknowledges that the U.S. Government retains a non-exclusive, paid-up, irrevocable, world-wide license to publish or reproduce the published form of this written work or allow others to do so, for U.S. Government purposes. The DOE will provide public access to results of federally sponsored research in accordance with the DOE Public Access Plan. Work at the University of Nottingham is supported by EPSRC (EP/V042556/1). We acknowledge the use of the Sulis supercomputer through the HPC Midlands+ Consortium, and the ARCHER2 supercomputer through membership of the UK's HPC Materials Chemistry Consortium, which are funded by EPSRC Grants No. EP/T022108/1 and No. EP/X035859/1, respectively.

References

(1) Yeh, J.-W.; Chen, S.-K.; Lin, S.-J.; Gan, J.-Y.; Chin, T.-s.; Shun, T.-T.; Tsau, C.-h.; Chang, S.-Y. Nanostructured high-entropy alloys with multiple principal elements: novel alloy design concepts and outcomes. *Adv. Eng. Mater.* **2004**, *6*, 299–303.

(2) Castle, E.; Csanádi, T.; Grasso, S.; Dusza, J.; Reece, M. Processing and properties of high-entropy ultra-high temperature carbides. *Sci. Rep.* **2018**, *8*, 8609.

(3) George, E.; Curtin, W.; Tasan, C. High entropy alloys: A focused review of mechanical properties and deformation mechanisms. *Acta Mater.* **2020**, *188*, 435–474.

(4) Sahlberg, M.; Karlsson, D.; Zlotea, C.; Jansson, U. Superior hydrogen storage in high entropy alloys. *Sci. Rep.* **2016**, *6*, 36770.

(5) Witman, M.; Ek, G.; Ling, S.; Chames, J.; Agarwal, S.; Wong, J.; Allendorf, M. D.; Sahlberg, M.; Stavila, V. Data-driven discovery and synthesis of high entropy alloy hydrides with targeted thermodynamic stability. *Chem. Mater.* **2021**, *33*, 4067–4076.

(6) Pasquini, L. et al. Magnesium- and intermetallic alloys-based hydrides for energy storage: modelling, synthesis and properties. *Prog. Energy* **2022**, *4*, 032007.

(7) Batchelor, T. A.; Pedersen, J. K.; Winther, S. H.; Castelli, I. E.; Jacobsen, K. W.; Rossmeisl, J. High-entropy alloys as a discovery platform for electrocatalysis. *Joule* **2019**, *3*, 834–845.

(8) Gao, M.; Zhang, C.; Gao, P.; Zhang, F.; Ouyang, L.; Widom, M.; Hawk, J. Thermodynamics of concentrated solid solution alloys. *Curr. Opin. Solid State Mater. Sci.* **2017**, *21*, 238–251.

(9) Zhang, J.; Liu, X.; Bi, S.; Yin, J.; Zhang, G.; Eisenbach, M. Robust data-driven approach for predicting the configurational energy of high entropy alloys. *Mater. Des.* **2020**, *185*, 108247.

(10) Yang, X.; Chen, S. Y.; Cotton, J. D.; Zhang, Y. Phase stability of low-density, multiprincipal component alloys containing aluminum, magnesium, and lithium. *JOM* **2014**, *66*, 2009–2020.

(11) Frenkel, D.; Smit, B., *Understanding molecular simulations*; Elsevier: San Diego, 2002.

(12) Sanchez, J.; Ducastelle, F.; Gratias, D. Generalized cluster description of multicomponent systems. *Phys. A Stat. Mech. its Appl.* **1984**, *128*, 334–350.

(13) Asta, M.; Wolverton, C.; De Fontaine, D.; Dreyssé, H. Effective cluster interactions from cluster-variation formalism. I. *Phys. Rev. B* **1991**, *44*, 4907–4913.

(14) Wolverton, C.; de Fontaine, D. Cluster expansions of alloy energetics in ternary intermetallics. *Phys. Rev. B* **1994**, *49*, 8627–8642.

(15) Feng, R.; Liaw, P. K.; Gao, M. C.; Widom, M. First-principles prediction of high-entropy-alloy stability. *npj Comput. Mater.* **2017**, *3*, 50.

(16) Rehman, T.; Jaipal, M.; Chatterjee, A. A cluster expansion model for predicting activation barrier of atomic processes. *J. Comput. Phys.* **2013**, *243*, 244–259.

(17) Li, C.; Nilson, T.; Cao, L.; Mueller, T. Predicting activation energies for vacancy-mediated diffusion in alloys using a transition-state cluster expansion. *Phys. Rev. Mater.* **2021**, *5*, 013803.

(18) Geng, H. Y.; Sluiter, M. H. F.; Chen, N. X. Cluster expansion of electronic excitations: Application to fcc Ni–Al alloys. *J. Chem. Phys.* **2005**, *122*, 214706.

(19) Das, P.; Thekkepat, K.; Lee, Y.-S.; Lee, S.-C.; Bhattacharjee, S. Computational design of novel MAX phase alloys as potential hydrogen storage media combining first principles and cluster expansion methods. *Phys. Chem. Chem. Phys.* **2023**, *25*, 5203–5210.

(20) Lun, Z. et al. Cation-disordered rocksalt-type high-entropy cathodes for Li-ion batteries. *Nat. Mater.* **2021**, *20*, 214–221.

(21) Spataru, C. D.; Witman, M. D.; Jones, R. E. Tuning the critical Li intercalation concentrations for MoX2 (X = S, Se, or Te) bilayer phase transitions. *Phys. Rev. Mater.* **2021**, *5*, 084005.

(22) Mueller, T.; Ceder, G. Bayesian approach to cluster expansions. *Phys. Rev. B* **2009**, *80*, 024103.

(23) Cao, L.; Li, C.; Mueller, T. The use of cluster expansions to predict the structures and properties of surfaces and nanostructured materials. *J. Chem. Inf. Model.* **2018**, *58*, 2401–2413.

(24) Natarajan, A. R.; Van der Ven, A. Machine-learning the configurational energy of multicomponent crystalline solids. *npj Comput. Mater.* **2018**, *4*, 56.

(25) Xie, T.; Grossman, J. C. Crystal graph convolutional neural networks for an accurate and interpretable prediction of material properties. *Phys. Rev. Lett.* **2018**, *120*, 145301.

(26) Park, C. W.; Wolverton, C. Developing an improved crystal graph convolutional neural network framework for accelerated materials discovery. *Phys. Rev. Mater.* **2020**, *4*, 063801.

(27) Chen, C.; Ye, W.; Zuo, Y.; Zheng, C.; Ong, S. P. Graph networks as a universal machine learning framework for molecules and crystals. *Chem. Mater.* **2019**, *31*, 3564–3572.

(28) Choudhary, K.; DeCost, B. Atomistic Line Graph Neural Network for improved materials property predictions. *npj Comput. Mater.* **2021**, *7*, 185.

(29) Unke, O. T.; Chmiela, S.; Gastegger, M.; Schütt, K. T.; Sauceda, H. E.; Müller, K.-R. SpookyNet: Learning force fields with electronic degrees of freedom and nonlocal effects. *Nat. Commun.* **2021**, *12*, 7273.

(30) Lupo Pasini, M.; Jung, G. S.; Irle, S. Graph neural networks predict energetic and mechanical properties for models of solid solution metal alloy phases. *Comput. Mater. Sci.* **2023**, *224*, 112141.

(31) Wen, M.; Horton, M. K.; Munro, J. M.; Huck, P.; Persson, K. A. A universal equivariant graph neural network for the elasticity tensors of any crystal system. *arXiv* **2023**, arXiv:2307.15242v1.

(32) Witman, M. D.; Goyal, A.; Ogitsu, T.; McDaniel, A. H.; Lany, S. Defect graph neural networks for materials discovery in high-temperature clean-energy applications. *Nat. Comput. Sci.* **2023**, *3*, 675–686.

(33) Chen, Z.; Andrejevic, N.; Smidt, T.; Ding, Z.; Xu, Q.; Chi, Y.-T.; Nguyen, Q. T.; Alatas, A.; Kong, J.; Li, M. Direct prediction of phonon density of states with euclidean neural networks. *Adv. Sci.* **2021**, *8*, 2004214.

(34) Choudhary, K.; DeCost, B.; Major, L.; Butler, K.; Thiyagalingam, J.; Tavazza, F. Unified graph neural network force-field for the periodic table: solid state applications. *Digit. Discov.* **2023**, *2*, 346–355.

(35) Deng, B.; Zhong, P.; Jun, K.; Riebesell, J.; Han, K.; Bartel, C. J.; Ceder, G. CHGNet as a pretrained universal neural network potential for charge-informed atomistic modelling. *Nat. Mach. Intell.* **2023**, *5*, 1031–1041.

(36) Youssef, K. M.; Zaddach, A. J.; Niu, C.; Irving, D. L.; Koch, C. C. A novel low-density, high-hardness, high-entropy alloy with close-packed single-phase nanocrystalline structures. *Mater. Res. Lett.* **2015**, *3*, 95–99.

(37) Ong, S. P.; Richards, W. D.; Jain, A.; Hautier, G.; Kocher, M.; Cholia, S.; Gunter, D.; Chevrier, V. L.; Persson, K. A.; Ceder, G. Python Materials Genomics (pymatgen): A robust, open-source python library for materials analysis. *Comput. Mater. Sci.* **2013**, *68*, 314–319.

(38) Aykol, M.; Dwaraknath, S. S.; Sun, W.; Persson, K. A. Thermodynamic limit for synthesis of metastable inorganic materials. *Sci. Adv.* **2018**, *4*, eaaq0148.

(39) Jain, A.; Ong, S. P.; Hautier, G.; Chen, W.; Richards, W. D.; Dacek, S.; Cholia, S.; Gunter, D.; Skinner, D.; Ceder, G.; Persson, K. A. Commentary: The Materials Project: A materials genome approach to accelerating materials innovation. *APL Mater.* **2013**, *1*, 011002.

(40) Chen, W.; Hilhorst, A.; Bokas, G.; Gorsse, S.; Jacques, P. J.; Hautier, G. A map of single-phase high-entropy alloys. *Nat. Commun.* **2023**, *14*, 2856.

(41) Ponsoni, J. B.; Aranda, V.; Nascimento, T. d. S.; Strozi, R. B.; Botta, W. J.; Zepon, G. Design of multicomponent alloys with C14 laves phase structure for hydrogen storage assisted by computational thermodynamic. *Acta Mater.* **2022**, *240*, 118317.

(42) Guan, P.-W.; Sun, Y.; Hemley, R. J.; Liu, H.; Ma, Y.; Viswanathan, V. Low-pressure electrochemical synthesis of complex high-pressure superconducting superhydrides. *Phys. Rev. Lett.* **2022**, *128*, 186001.

(43) Flanagan, T. B.; Luo, S. Thermodynamics of hydrogen solution and hydride formation in binary pd alloys. *J. Phase Equilibria Diffus.* **2007**, *28*, 49–57.

(44) Hautier, G.; Ong, S. P.; Jain, A.; Moore, C. J.; Ceder, G. Accuracy of density functional theory in predicting formation energies of ternary oxides from binary oxides and its implication on phase stability. *Phys. Rev. B* **2012**, *85*, 155208.